Using the Suess effect on the stable carbon isotope to distinguish the future from the past in radiocarbon

Environmental Research Letters

OPEN ACCESS

RECEIVED
6 September 2016

REVISED
16 November 2016

ACCEPTED FOR PUBLICATION
18 November 2016

PUBLISHED
7 December 2016

LETTER

Using the Suess effect on the stable carbon isotope to distinguish the future from the past in radiocarbon

Peter Köhler

Alfred-Wegener-Institut Helmholtz-Zentrum für Polar-und Meeresforschung (AWI), PO Box 12 01 61, D-27515 Bremerhaven, Germany

E-mail: Peter.Koehler@awi.de

Keywords: carbon cycle, future CO_2 emissions, carbon isotopes, radiocarbon dating, Suess effect, modeling, carbon dioxide removal

Supplementary material for this article is available online

Abstract

The depletion of ^{14}C due to the emission of radiocarbon-free fossil fuels (^{14}C Suess effect) might lead to similar values in future and past radiocarbon signatures potentially introducing ambiguity in dating. I here test if a similar impact on the stable carbon isotope via the ^{13}C Suess effect might help to distinguish between ancient and future carbon sources. To analyze a wide range of possibilities, I add to future emission scenarios carbon dioxide reduction (CDR) mechanisms, which partly enhance the depletion of atmospheric $\Delta^{14}C$ already caused by the ^{14}C Suess effect. The ^{13}C Suess effect leads to unprecedented depletion in $\delta^{13}C$ shifting the carbon cycle to a phase space in $\Delta^{14}C$–$\delta^{13}C$, in which the system has not been during the last 50 000 years and therefore the similarity in past and future $\Delta^{14}C$ (the ambiguity in ^{14}C dating) induced by fossil fuels can in most cases be overcome by analyzing ^{13}C. Only for slow changing reservoirs (e.g. deep Indo-Pacific Ocean) or when CDR scenarios are dominated by bioenergy with capture and storage the effect of anthropogenic activities on ^{13}C does not unequivocally identify between past and future carbon cycle changes.

1. Introduction

One of the side effects of anthropogenic CO_2 emissions is the so-called (^{14}C) Suess effect (Suess 1955), the depletion of the radiocarbon isotopic signature of atmospheric CO_2 due to the injection of large amounts of ^{14}C-free fossil fuels (Stuiver and Quay 1981). It has been shown with models (Caldeira *et al* 1998, Graven 2015) that by the end of the 21st century for most emission scenarios atmospheric $\Delta^{14}C$ might be smaller than $\Delta^{14}C$ in surface and intermediate oceanic water masses. This would reverse the past and present day atmosphere-to-ocean gradient in $\Delta^{14}C$ and complicate conventional radiocarbon dating. For example, from the year 2050 onward fresh organic material might have the same $^{14}C/^{12}C$ ratio as samples from 1050 CE and earlier, making both past and future samples indistinguishable if analyzed by radiocarbon dating alone (Graven 2015).

Not yet mentioned in this previous analysis (Graven 2015) is the fact that ^{13}C is also affected by anthropogenic CO_2 emissions, since most of the released carbon has its origin in organic material, in which ^{13}C is depleted with respect to ^{12}C due to isotopic fractionation during photosynthesis (Lloyd and Farquhar 1994). Charles Keeling named this the *^{13}C Suess effect* (Keeling 1979), which has since then been widely observed in carbon reservoirs, e.g. in the atmosphere (Rubino *et al* 2013) and the surface ocean (Gruber *et al* 1999, Swart *et al* 2010, Schmittner *et al* 2013).

To project how emissions and therefore the Suess effects might develop in the future the international commitments to act against ongoing anthropogenic emissions need to be considered. Climate negotiations during the 21st Conference of Parties of United Nations Framework Convention on Climate Change in December 2015 in Paris have strengthened the political will to keep global warming caused by mankind under some agreed-upon thresholds (Iyer *et al* 2015), whose details are still a matter of debate (Knutti *et al* 2016). To meet such global warming thresholds, and to operate against a likely CO_2 overshoot, not only a reduction in fossil fuel emissions (Rogelj *et al* 2013),

but also some active CO_2 removal from the atmosphere might be necessary (Smith *et al* 2016b) in order to achieve net zero emissions on the long-term (Rogelj *et al* 2015). Furthermore, once net zero emissions are achieved the rebound effect (Cao and Caldeira 2010), the outgassing of anthropogenic CO_2 previously taken up by the ocean, might also urge mankind to implement negative CO_2 emissions or carbon dioxide reduction (CDR) mechanisms in order to keep atmospheric CO_2 at the desired concentration.

Model-based analysis of various CDR approaches are the subject of ongoing research. Within the most recent assessment of CDR (Smith *et al* 2016b) various different approaches have been compared with respect to their requirements in terms of energy, land, nutrient and water usages, their impacts on albedo and their costs. One of the CDR approaches analyzed in that study (bioenergy (BE) with carbon capture and storage (CCS), combined to BECCS) has already been implemented in some of the Representative Concentration Pathway (RCP) emission scenarios used for the most recent IPCC report (Meinshausen *et al* 2011, van Vuuren *et al* 2011). The magnitude of BECCS was up to 3.1, 1.2 and 0.2 PgC yr^{-1} in RCP2.6, RCP4.5 and RCP6.0, respectively, compensating for some of the fossil fuel emissions and leading in RCP2.6 to negative CO_2 emissions at the end of this century (figure 1(A) inlet).

I will here have a look at potential changes in the carbon isotopes in the future and analyze how the ^{13}C Suess effect might help to solve the proposed future radiocarbon dating conundrum caused by the ^{14}C Suess effect. For this aim I will extend the analysis of the emission scenarios to the year 2500 using the well tested carbon cycle box model BICYCLE (Köhler *et al* 2005), which is described in detail in the supplementary material. The extensions of the RCP emissions scenarios beyond the year 2100 were labeled the Extended Concentration Pathways (ECPs) (Meinshausen *et al* 2011). However, for reasons of simplicity I here address the emission scenarios as 'RCP', no matter if it concerns changes until or after the year 2100. I will also incorporate how the carbon cycle might be further affected by some CDR methods discussed nowadays to cover an as wide as possible range of potential changes in ^{13}C and ^{14}C. Finally, I set the simulated future dynamics in the carbon isotopes into perspective of what is known from paleo data (and modeling) covering the last 50 000 years.

2. Simulation scenarios

I use the historical anthropogenic carbon release (1765–2005) from both fossil fuel emissions (including cement production) and land use changes

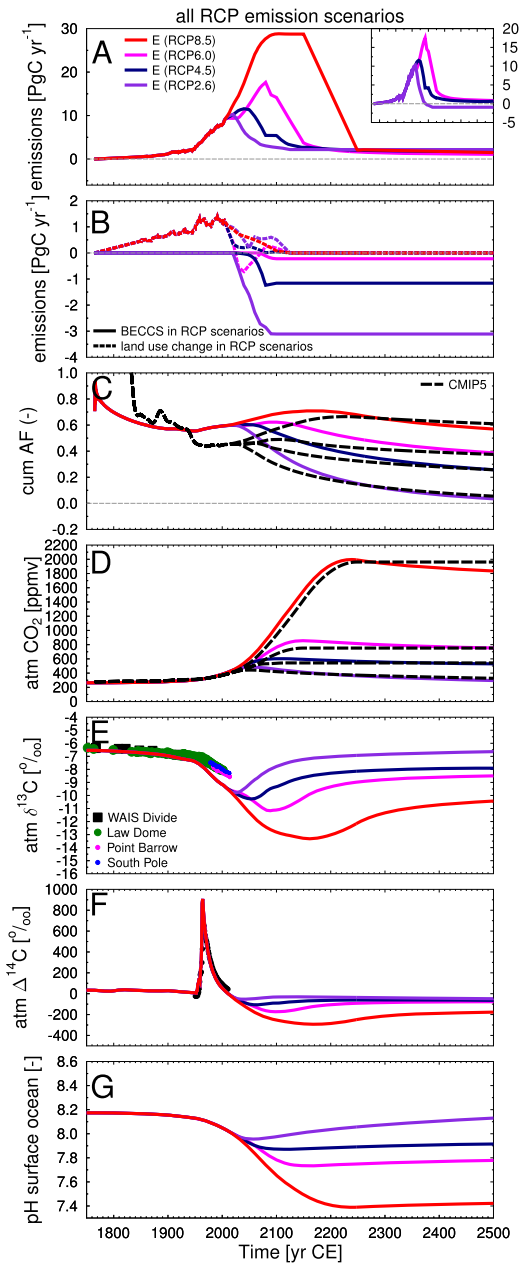

Figure 1. Future carbon cycle simulation results until year 2500 for all four emission scenarios (RCP2.6, RCP4.5, RCP6.0, RCP8.5) (Meinshausen *et al* 2011). (A) Total anthropogenic emissions rates E (sum of fossil fuel and land use change emissions). Net emissions (E–BECCS in PgC yr^{-1}) for RCP2.6, RCP4.5, RCP6.0 are shown in the small inlet. (B) Contributions of land use change emissions to and prescribed CDR via BECCS already contained in the respective RCP scenarios. (C) Cumulative airborne fraction (AF): $\Delta A/\sum E$ with ΔA change in atmospheric C content and $\sum E$ the cumulative sum of emissions. (D) Simulated atmospheric CO_2, black broken lines are the past reconstruction of CO_2 (instrumental at Mauna Loa) (Keeling and Whorf 2005) and Law Dome ice core (Rubino *et al* 2013) or the mean of projected future concentrations of emission driven simulations within CMIP5 for the different RCP scenarios (Meinshausen *et al* 2011); (E) Simulated atmospheric $\delta^{13}C$ and reconstructions (instrumental: Point Barrow, South Pole, Keeling *et al* 2001, ice cores: Law Dome and WAIS Divide, Rubino *et al* 2013, Bauska *et al* 2015); (F) Simulated atmospheric $\Delta^{14}C$ including in black the reconstructed radiocarbon bomb peak (Hua *et al* 2013); (G) Simulated mean pH of the surface ocean.

(figure S1A) as contained in the extended version of the RCP emission scenarios (Moss *et al* 2010, Meinshausen *et al* 2011), which proposed carbon emissions from 2006 onward until the year 2500 (figure 1(A)). The historical emission fluxes contained in the RCP scenarios (Meinshausen *et al* 2011) are slightly smaller in the 2nd half of the 20th century than in those previously published (Houghton 2003) due to some downward correction of the land use emission fluxes. Assumptions then have to be made on the isotopic signature of the emissions (figure S1B): the $\delta^{13}C$ signature of fossil emissions is taken from reconstructions between 1765 and 2011 and kept constant at its 2011 value thereafter (Andres *et al* 2000, 2015), while that from land use change is internally calculated from the atmospheric $\delta^{13}C$ value using the isotopic fractionation during C_3 photosynthesis by −19‰. Similarly, the ^{14}C signature from land use emissions is derived using twice the named isotopic fractionation for $\delta^{13}C$, while fossil fuels are assumed to contain no ^{14}C. I only consider CO_2 emissions, all other anthropogenic emissions contained in the RCP scenarios are neglected.

The ^{14}C production rate is prescribed before 1950 CE (Roth and Joos 2013) varying around a mean production rate of 440 mol per year, kept constant thereafter with individual years in the 1950ies to 1970ies with high peaks in ^{14}C production caused by nuclear bomb testing (Naegler and Levin 2006) (figure S1C). Potential impacts of ^{14}C production from the nuclear industry (Graven and Gruber 2011, Graven 2015) are tested with sensitivity runs (see supplementary material for details on ^{14}C production rate). All simulations are started in year 10 000 BP to allow the ^{14}C cycle to adjust to variable production rates.

For model evaluation (supplementary material) the simulated time series of atmospheric CO_2, $\delta^{13}C$ and $\Delta^{14}C$ are then compared with historical data from both ice cores and instrumental records (figure S2), but also with the proposed atmospheric CO_2 concentrations of the RCP emission scenarios (Moss *et al* 2010, Meinshausen *et al* 2011) that should be taken as radiative forcing time series in the CMIP5 model intercomparison project.

Additionally I investigate three different methods of CDR, (a) bioenergy with capture and storage (BECCS), (b) direct air capture (DAC), and (c) ocean alkalinization or enhanced weathering (EW), which all interact with the carbon cycle in completely different ways. I prescribe the strength of these three methods in order to linearly reduce net carbon emissions from 2021 onward until an annual net removal of 5 Pg C yr^{-1} is achieved in the year 2050, and maintained thereafter. Alternatively, after year 2070 the 5 Pg C yr^{-1} net CO_2 removal would cease (scenarios BECCSs, DACs and EWs), and the simulations would continue. In DAC carbon is extracted from the atmospheric pool and assumed to be permanently stored in some geological reservoir without any further exchange with the atmosphere-ocean-terrestrial biosphere subsystem of the carbon cycle. The storage is similar in BECCS, but the extraction of carbon is based in biologically produced organic carbon, implying that isotopic fractionation during photosynthesis took place first, having a net effect on the carbon isotopes, and making BECCS similar to a land use change scenario with negative emissions. In EW an enhanced weathering or ocean alkalinization flux is calculated that approximates the desired CO_2 removal: 1 mol of desired CO_2 removal triggers the input of 1 mol of bicarbonate ion (HCO_3^-) into the surface ocean, which would be the product of any man-made EW by enhanced silicate weathering that changes both the carbon content and the alkalinity in the ocean and ultimately the CO_2 uptake capacity of the world oceans. In practical terms the molar input of HCO_3^- can be related to the necessary amount of silicate rocks that needs to be dissolved by the relevant net chemical dissolution equations, e.g. 1 g of olivine (Mg_2SiO_4 with about 140 g mol^{-1}) would lead to a theoretical input of $1/140 \times 4 = 0.03$ mol of HCO_3^- (for details see Köhler *et al* 2010, Griffioen 2016). Any second order effects of enhanced silicate rock weathering that might occur due to changes in the biological pump (Köhler *et al* 2013, Hauck *et al* 2016) are ignored here.

The isotopic signature of fluxes related to BECCS, DAC and EW are consistently calculated within the model: both the CO_2 extracted within BECCS and DAC and the influx of HCO_3^- into the surface ocean during EW contain the $\delta^{13}C$ and $\Delta^{14}C$ signatures of the atmospheric reservoir during the relevant time step (additionally within BECCS isotopic fractionation by −19‰ due to photosynthesis is considered). The differences in the isotopic signatures of the RCP and CDR fluxes are the reason why both the emission and the CO_2 removal fluxes need to be prescribed individually, and not only as one net flux. The size of BECCS as assumed in RCP2.6, RCP4.5, and RCP6.0 in the 21st century is assumed to stay constant on its 2100 level thereafter (figure 1(B)).

3. Results and discussions

My discussion of carbon cycle results is focused on the RCP8.5 emission scenario and subsequent CDR approaches diverging from it. However, the results for the other scenarios (RCP2.6, RCP4.5, RCP6.0) are included in the figures and the effects on the carbon isotopes in them is contained in my analysis of the combined Suess effects.

3.1. Carbon cycle dynamics

In the RCP8.5 emission scenario mitigation efforts start late leading to anthropogenic emission rates of up to nearly 30 Pg C yr^{-1} around year 2100 with an assumed linear reduction between 2150 and 2200 to a constant emission rate of 1.5 Pg C yr^{-1} until year

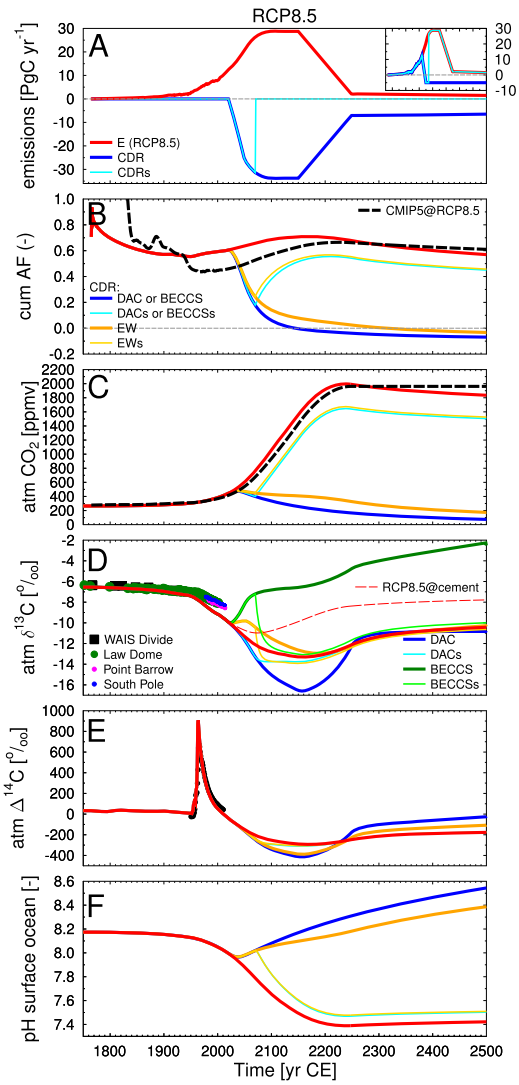

Figure 2. Carbon cycle simulation results from pre-industrial times until year 2500. Results are based on RCP8.5 emission scenario (Meinshausen *et al* 2011) including carbon dioxide reduction (CDR) via bioenergy and carbon capture and storage (BECCS), direct direct air capture (DAC) and enhanced weathering (EW). BECCS and DAC differ only in δ^{13}C, changes in Δ^{14}C are on the order of a few permil only and negligible. (A) Emission rate E of RCP8.5 in the extended scenario until 2500 and the negative emissions of CDR approaches. Small inlet sketches the net emissions (E–CDR in PgC yr^{-1}). (B) Cumulative airborne fraction (AF): $\Delta A/\sum E$ with ΔA change in atmospheric C content and $\sum E$ the cumulative sum of emissions. (C) Simulated atmospheric CO_2, black broken line is the past reconstruction of CO_2 (instrumental at Mauna Loa) (Keeling and Whorf 2005) and Law Dome ice core (Rubino *et al* 2013) or the mean of projected future concentrations within CMIP5 for RCP8.5 (Meinshausen *et al* 2011); (D) Simulated atmospheric δ^{13}C and reconstructions (instrumental: Point Barrow, South Pole, Keeling *et al* 2001, ice cores: Law Dome and WAIS Divide, Rubino *et al* 2013, Bauska *et al* 2015). RCP8.5@cement is a sensitivity study in which the source of the fossil fuel emission is slowly shifting from today 6% to 100% cement in year 2250. Cement has a δ^{13}C signature of 0‰. (E) Simulated atmospheric Δ^{14}C including in black the reconstructed radiocarbon bomb peak (Hua *et al* 2013). (F) Simulated mean *p*H of the surface ocean.

2500. (figure 2(A)). These emissions would result in a rise in atmospheric CO_2 concentration from present day 400 ppmv to ~2000 ppmv after year 2200 in both the CMIP5 scenarios (Meinshausen *et al* 2011) and my carbon cycle simulations (figure 2(C)). The global warming and ocean acidification connected with such a rise in the most important anthropogenic greenhouse gas would be severe leading in my simulations to a temperature rise of 5–6 K (figure S3) and a drop in mean surface ocean pH by 0.8 units (from 8.2 to 7.4) (figure 2(F) inlet).

Within the hypothetical CDR scenarios investigated here, net emissions are reduced even faster than in the other RCP emission scenarios assuming negative net emissions from year 2040 onward (figure 2(A)) and therefore broaden the range of possible future scenarios. The carbon extraction achieved in these CDR simulations might be unrealistically high, however, my interest here lies in showing potential maximum impacts on the carbon isotopes and not to investigate the most plausible scenario.

The cumulative airborne fraction (AF) of the anthropogenic emissions E (Pg C yr^{-1}), here defined as the ratio in the difference in atmospheric carbon pool (with respect to the pre-industrial values in year 1765) over the cumulative sum of E, stays in my simulations around 0.6 (figure 2(B)). Cumulative AF calculated from emission driven CMIP5 data are before year 1830 larger than 1, probably due to carbon cycle internal variability not driven by the yet small anthropogenic emissions. In the 21st and 22nd centuries they are slightly smaller than in my simulations. This difference is explained with the passive (=constant) terrestrial carbon pools in my simulations which neglects the terrestrial carbon sink found in the historical data (Le Quéré *et al* 2015). I refrain from showing results with active (=variable) terrestrial carbon cycle, since for atmospheric CO_2 concentrations well above 500 ppmv, the CO_2 fertilization implemented in my simple model is much too large, when compared with CMIP5 models, leading, due to the massive buildup of terrestrial carbon, to unrealistically low atmospheric CO_2 concentration (Köhler *et al* 2015). I here restrict simulation results to those obtained with an atmosphere-ocean only setup of the the carbon cycle, which on the long run agree in the atmospheric carbon pools with those of the CMIP5 results, although the still existing uncertainty in the land carbon cycle, partly due to an overestimation of the CO_2 fertilization (Smith *et al* 2016a), or due to uncertainties in the nitrogen cycle (Meyerholt *et al* 2016) might indicate that CMIP5 results are also not perfect. On the long run the cumulative AF and atmospheric CO_2 of my simulations converge with those based on CMIP5, indicating a small long-term influence of the terrestrial carbon sink in models contributing to CMIP5 (figures 1(C) and 2(B)). Simulations including terrestrial carbon storage changes would result in smaller simulated atmospheric CO_2, smaller AFs, and less depleted atmospheric δ^{13}C. Therefore, the historical ^{13}C Suess effect is better matched by using an active terrestrial carbon cycle (figure S2B), while the effect on the historical ^{14}C Suess effect reduces the offset

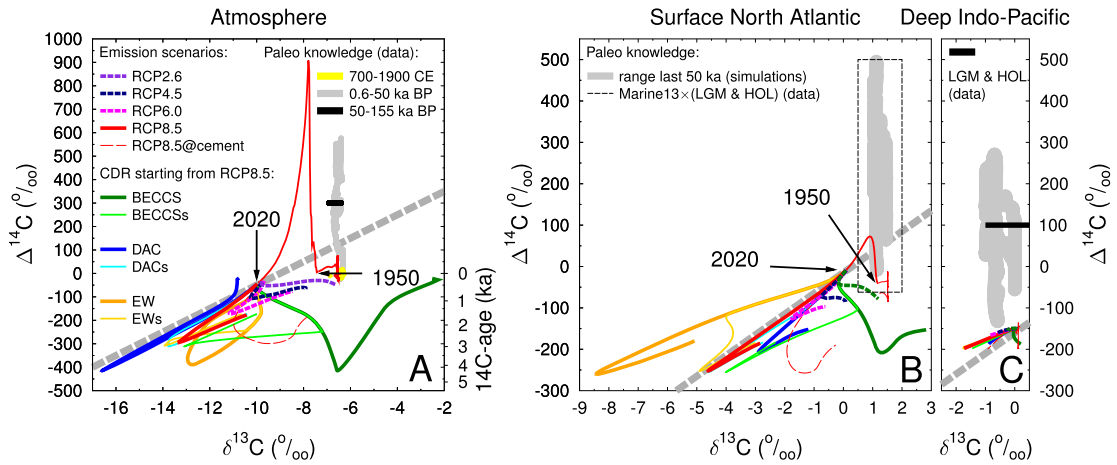

Figure 3. Analysis of the combined Suess effects on both ^{14}C and ^{13}C. Scatter plot of simulated $\Delta^{14}C$ versus $\delta^{13}C$ (A) atmosphere, (B), (C): end-members within the ocean (surface North Atlantic, deep Indo-Pacific) showing the historical and future Suess effects and the influence of bomb-^{14}C, future CO_2 emissions and carbon dioxide reduction (CDR) approaches (BECCS, DAC, EW) on both variables. Also included in dotted lines are results for RCP2.6, RCP4.5 and RCP6.0, which all contain a prescribed contribution of BECCS (see figure 1 for details). The right *y*-axis in panel (A) also provides, similarly as before in Graven 2015, a conventional calculated ^{14}C-age $= 8033 \times \ln(\Delta^{14}C/1000 + 1)$ for all $\Delta^{14}C$ values below zero (1 ka = 1000 years). For comparison, also the available paleo knowledge is added: (A) Atmospheric $\delta^{13}C$ from ice cores (700–1900 CE: WAIS Divide ice core, Bauska *et al* 2015; further back in time: spline through ice core compilation, Eggleston *et al* 2016) and $\Delta^{14}C$ from IntCal13 (Reimer *et al* 2013), for 50–155 ka BP plotted with fixed $\Delta^{14}C = 300‰$; In the ocean I show the data range obtained from sediment cores in $\delta^{13}C$ (Peterson *et al* 2014) obtained for the Last Glacial Maximum (LGM) and the late Holocene (HOL) for (B) the range of surface ocean $\Delta^{14}C$ contained in Marine13 (Reimer *et al* 2013) or (C) for a fixed value of $\Delta^{14}C = 100‰$. Additionally, the range in both isotopes in previously published (imperfect) simulations using the BICYCLE model covering the last 50 000 year (50 ka) is shown (upper limit of scenario S3x (^{14}C production rate based on ^{10}Be) and lower limit of scenario S4x (^{14}C production rate based on reconstructions of the geomagnetic field strength GLOPIS-75) as used before in Köhler *et al* 2006). The gray broken line in all subplots crosses values for year 2020 with a slope $m = 50$ (see text for further explanation).

between model and data, but has negligible impact on the ^{14}C dynamic (figure S2C).

All CDR methods have a permanent impact on atmospheric CO_2 concentrations and on surface ocean pH (figures 2(C), (F)). Even in the scenarios BECCSs, DACs and EWs, in which CDR is stopped after some decades (here in year 2070) the simulated CO_2 concentrations (and surface ocean pH) do not reach the values obtained without CDR. The assumed CDR scenarios would eventually lead to a cumulative AF of zero, implying that an amount of CO_2 identical to the sum of all anthropogenic CO_2 emissions has been extracted from the carbon cycle again and atmospheric CO_2 concentration starts to fall below pre-industrial values.

3.2. Carbon isotopes: the ^{14}C and ^{13}C Suess effects

The carbon isotopes of atmospheric CO_2 are both depleted by the massive injection of anthropogenic emissions, since fossil fuels are ^{14}C-free and contain with about −24 to −29‰ a $\delta^{13}C$ signature (Andres *et al* 2000, 2015) that is 19‰ lighter than the $\delta^{13}C$ signature of the atmospheric CO_2 itself (figure S1B). Additionally, the radiocarbon cycle is penetrated by the bomb-^{14}C emissions in the second half of the last century (Naegler and Levin 2006) leading around 1965 to atmospheric $\Delta^{14}C$ values of up to +700 ± 200‰ in the data (Hua *et al* 2013) and of +900‰ in my simulations (figure 2(E)) (see supplementary material for further details).

Atmospheric $\Delta^{14}C$ then drops around 2150 to −300‰ in RCP8.5 and to −415‰ in all CDR approaches. This most depleted $\Delta^{14}C$ signature of −415‰ is identical to that of a 4300 year old carbon sample (figure 3(A)). Depending on the assumed CDR method $\delta^{13}C$ of atmospheric CO_2 drops at the same time to values of (RCP8.5) −13.3‰, (EW) −12.6‰, or (DAC) −16.6‰ (figure 2(D)). For BECCS $\delta^{13}C$ of atmospheric CO_2 returns to its pre-industrial value of −6.5‰ in year 2150 and rises thereafter to values up to −2‰. Here, the difference of how the CDR methods modify the carbon cycle has a significant impact on the resulting atmospheric $\delta^{13}C$ signature: BECCS operates as negative land use change, therefore reversing the ^{13}C Suess effect. In scenario EW alkalinity is added to the ocean. The isotopic fractionation within the dissolved inorganic carbon (DIC) in the ocean and therefore of the ocean-atmosphere gas exchange depends directly on the concentration of HCO_3^- and CO_3^{2-}, two of the chemical species of DIC. However, the concentrations of these species change with a rise in alkalinity to allow a larger oceanic CO_2 storage. Therefore, the isotopic fractionation during gas exchange indirectly depends on the surface ocean alkalinity (Zeebe and Wolf-Gladrow 2001) and is in detail implemented in BICYCLE similarly as in other models (Ridgwell 2001).

When $\Delta^{14}C$ and $\delta^{13}C$ are plotted against each other it clearly becomes evident that the Suess effects on both isotopes will in the future bring the isotopic

carbon cycle into a regime in which it has not been during at least the last 50 000 years. The historical Suess effect before 1950 (−0.7‰ in δ^{13}C and −20‰ in Δ^{14}C) already shifted the atmospheric variables away from its natural state (figure 3(A)). The atmospheric Δ^{14}C simulated in response to the bomb-^{14}C injection led to 0 to +900‰, slightly larger than the range of −25-to- +575‰ that has been reconstructed for the pre-industrial 50 000 years from various archives (Köhler *et al* 2006, Reimer *et al* 2013). Already the historical emissions from 1950 onward including the foreseeable emissions until 2020 shift the atmospheric δ^{13}C by another −2‰. In most scenarios a further depletion in both carbon isotopes takes place in the near future. At the extreme, values of $\Delta^{14}C = -415‰$ and $\delta^{13}C = -16.6‰$ are reached in the atmospheric carbon reservoir. The exceptions to this rule are scenarios in which BECCS plays a dominant role, also implying that RCP2.6 has a different dynamic in the carbon isotopes than the other RCP scenarios. EW would first lead to a small rise in δ^{13}C but on the long run also to a depletion. In BECCS the simulated δ^{13}C on the long run is higher than what is known from the paleo record. Most scenarios might, after having a maximum depletion in the isotopic phase space, return to less extreme anomalies in both isotopes, only RCP2.6 returns in the Δ^{14}C–δ^{13}C-scatter plot back to conditions seen in pre-industrial times or found in the paleo simulations or reconstructions.

To analyze how the carbon isotopes in the ocean might change due to the Suess effects I focus on the two end-member in the oceanic carbon cycle: (a) North Atlantic surface waters, where North Atlantic Deep Water formation occurs and a dominant part of deep ocean water masses have last contact with the atmosphere and (b) the deep Indo-Pacific, in which the oldest, most Δ^{14}C-depleted water masses are found. A similar pattern as found in the atmosphere emerges in the North Atlantic surface waters, although with smaller amplitude (figure 3(B)): the bomb-^{14}C spike is found with slightly more than +100‰, the ^{13}C Suess effect leads until 2020 to a reduction in δ^{13}C by nearly −1.5‰, and all scenarios but RCP2.6 enter uncharted waters in the Δ^{14}C–δ^{13}C phase space. Clearly seen is also that the rising ocean alkalinity in the EW CDR method leads to a more depleted surface ocean δ^{13}C, explaining the lower isotopic fractionation (less depletion) in the atmospheric δ^{13}C record and the special dynamics for BECCS leading to δ^{13}C of nearly +3‰. An overlap of the historical and future simulations with the data range spanned by paleo data (Reimer *et al* 2013, Peterson *et al* 2014) and paleo simulations (Köhler *et al* 2006) covering the last 50 000 years is only obtained for the bomb-^{14}C spike. Also note, that these paleo simulations, performed with a previous version of the same model, were imperfect, since they were not able to explain the full decline in atmospheric Δ^{14}C found in the paleo reconstructions (Reimer *et al* 2013).

The simulated changes in the deep Indo-Pacific during the next five centuries are much smaller than for the surface ocean (figure 3(C)). Until 2020 the Suess effects or even the ^{14}C-bomb spike are not detectable in this reservoir, however the effect of further anthropogenic emissions will over the course of the simulations found its way to this most remote ocean reservoir and both Suess effects will then be visible there. The simulated future trends in the deep Indo-Pacific δ^{13}C have some overlap with the range of reconstructed δ^{13}C, however, the knowledge on deep ocean Δ^{14}C is still limited. While my previous (imperfect) simulations suggest that deep Indo-Pacific Δ^{14}C was always higher than −150‰ throughout the last 50,000 years, the limited available deep ocean Δ^{14}C reconstructions show a different picture (Ronge *et al* 2016): Δ^{14}C-values as low as −200‰ are found in waters above 2000 m and below 4300 m water depth in the South Pacific with some water masses in between (and in intermediate depths of ~600 m around the Galapagos Islands (Stott *et al* 2009) having during the last 25 000 years a Δ^{14}C signature as low as −600‰. This would imply that for most of the RCP emission scenarios the deep Pacific data in the Δ^{14}C–δ^{13}C phase space might already have been obtained in some form during glacial conditions in the past. These most recent deep Pacific data with low Δ^{14}C signature (Ronge *et al* 2016) are not yet completely understood. It is not yet clear how wide-spread this water mass is and the explaining hypothesis put forward so far suggests the release of ^{14}C-free CO_2 from hydrothermal activities along mid-ocean ridges during sea-level low stand in glacial times. This would imply that the deep glacial ocean would contain, in addition to the fossil fuel emissions into the atmosphere, another source of ^{14}C-free carbon. The interpretation of deep ocean carbon isotopic signatures might therefore be not yet straightforward.

Simulation results for other surface ocean reservoirs are qualitatively similar to the North Atlantic surface end member discussed in detail above (figure S4), allowing in surface reservoirs to use the ^{13}C Suess effect to distinguish past from future carbon fluxes. Interestingly, the largest oceanic anomalies in δ^{13}C are obtained in the surface equatorial Atlantic Ocean (figure S4B) with δ^{13}C falling down to −13‰ for EW scenarios, probably caused by the way the EW fluxes are prescribed. These fluxes enter the surface ocean only in the equatorial regions, with 50% each routed in the Atlantic and Indo-Pacific. Combined with the smaller size of the Atlantic basin, the effect of EW on the local carbon cycle is more pronounced in the Atlantic than in the Indo-Pacific. Since the prescribed water mass fluxes to the surface North Pacific area are all sourced in deep ocean regions, δ^{13}C in this area follows in the EW scenarios the dynamics seen in the atmosphere (less depleted than in RCP8.5, figure S4F). Carbon isotopic dynamics in the deep ocean of the

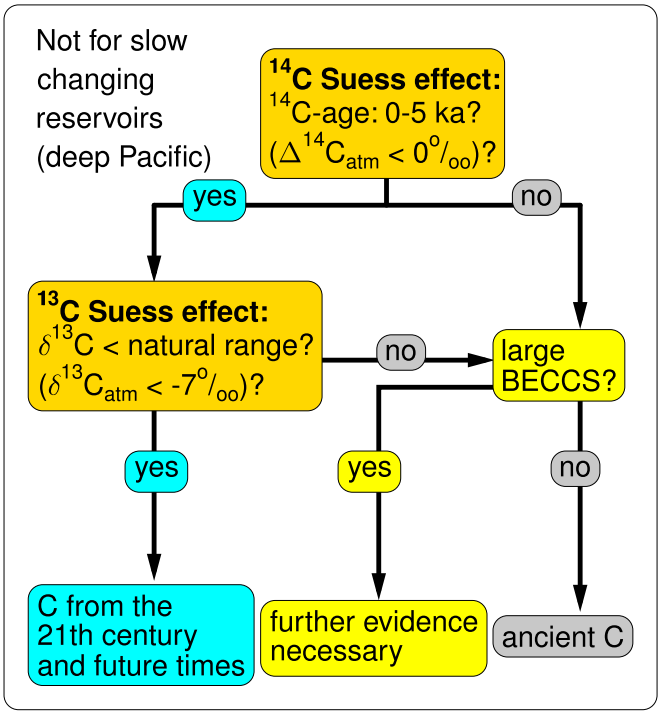

Figure 4. Decision tree how to distinguish ancient carbon from carbon which requires an age marker from future times. The combination of radiocarbon dating and how δ^{13}C needs to leave its natural range due to the combined ^{14}C and ^{13}C Suess effects with examples for the atmospheric reservoir are given. For cases in which CDR by a large contribution of BECCS is realized (e.g. as in RCP2.6) the carbon isotopic signatures might return back to pre-industrial values. For these cases further not yet identified evidence is necessary to distinguish ancient from future carbon. For slow changing reservoirs, e.g. the deep Pacific, changes for the future overlap with past data ranges, so a clear identification of ancient versus future carbon is not possible.

Atlantic (figure S4C) and to some extend in the Southern Ocean (figure S4E) depart from known data ranges in the past. My approach to disentangle past from future carbon cycle changes therefore seemed also to be applicable to data from these deep ocean reservoirs. Further regional details are better obtained with spatially higher resolved models.

Fossil fuel fluxes contain also emissions from industrial processes, namely cement production. The δ^{13}C signature of fossil fuels therefore depends on the source mix and ranges from 0‰ (cement production) to −44‰ (natural gas) (Andres *et al* 2000). About 6% of the CO_2 emissions summarized as fossil fuels in year 2014 have been from cement production (Le Quéré *et al* 2015). In my standard scenarios I assume that the source mix (and therefore the δ^{13}C signature of fossil fuels) remains the same from year 2011 onward. In one scenario (RCP8.5@cement) I test the effect when cement production would slowly become the one and only source of the fossil fuel emissions in year 2250 (evolution of δ^{13}C of fossil fuels shown in figure S1B). Simulated δ^{13}C values would then be less depleted than in our standard simulations (figure 2(D)), but isotopic values would still be outside of their ranges known from the past (figure 3), and the overall conclusion would therefore not be affected by such a rise in the relative importance of cement in the source mix of future fossil fuel emissions.

4. Conclusions

When considering not only the ^{14}C Suess effect but also the ^{13}C Suess effect the future changes in the carbon isotopes in the atmosphere and the neighboring reservoirs (surface ocean, to some extend relatively fast ventilated water masses of the deep ocean, but also terrestrial biosphere) follow a distinct pattern that makes them distinguishable from variability in the past. This study is after the initial modeling study (Keeling 1979) one of a few approaches (e.g. Jahn *et al* 2015) in which both Suess effects are considered together. Simulation studies typically focus on either the ^{14}C Suess effect (Caldeira *et al* 1998, Graven 2015) or ^{13}C Suess effect (Gruber *et al* 1999, Tagliabue and Bopp 2008, Schmittner *et al* 2013). Changes in the carbon isotopic signature can be approximated from theory by considering that the injection of ^{14}C-free fossil fuels with a δ^{13}C signature of −28‰ leads to a carbon influx that differs from the present day atmosphere by $\Delta(\Delta^{14}C) \approx -1000‰$ and $\Delta(\delta^{13}C) \approx -20‰$. These differences are equivalent to a linear change with a slope $m = -1000‰/-20‰ = 50$ in the Δ^{14}C–δ^{13}C phase space as indicated by the broken lines in figures 3 and S4. The realized simulations that do not contain CDR due to BECCS or EW, nearly meet this theoretical expectation.

I therefore propose that measuring ^{13}C in parallel to ^{14}C measurements will enable researchers to distinguish

the future from the past in radiocarbon. This approach should be applicable for carbon reservoirs that are in reasonable fast exchange with the atmosphere to allow any Suess effect to be visible in the data sets. For data from deep ocean sites, especially from the Indo-Pacific, the observed future variability in the carbon isotopes might be too small to identify a clear excursion from past data ranges. If a ^{14}C-age falls within the range of 0 to 5000 years (corresponding to Δ^{14}C in the atmosphere of approximately 0 to −450‰) a cross-check on the ^{13}C Suess effect is necessary (figure 4). Here, isotopic fractionation during photosynthesis needs to be taken into account, if the relevant probe was derived for organic carbon. If the carbon cycle has been heavily perturbed by both Suess effects, the probe has its origin (age) within this or future centuries. If no ^{13}C Suess effect can be detected then the relevant carbon is of ancient origin, e.g. it had its last contact with the atmosphere in the past before fossil fuels perturbed the carbon cycle. For the exception that a large contribution of CDR is obtained via BECCS further evidences might be necessary since the carbon cycle might then not leave the Δ^{14}C–δ^{13}C-space known from historical and paleo reconstructions. I am aware that this isotopic fractionation during photosynthesis depends on various factors and might itself lead to a wide range of δ^{13}C within any organic material (Lloyd and Farquhar 1994), even without any perturbations of the ^{13}C Suess effect. Therefore, expert knowledge on the expected natural range of δ^{13}C within the any organic material is certainly necessary to make this final conclusion.

Earth system models contributing to CMIP5 including an active terrestrial biosphere might reduce uncertainties in the simulated future carbon cycle dynamics. The general pattern found here with a simplified carbon cycle model that the ^{13}C Suess effect might be used to distinguish between past and future carbon sources, however, is robust and should not change if investigated with more complex models.

Acknowledgments

The design of the CDR scenarios was motivated by initially proposed scenarios within the CDR-MIP project. Thanks to the RCP core group and Heather Graven for providing data on the amplitude of BECCS within the RCP scenarios. I thank Dieter Wolf-Gladrow and Gregor Knorr for helpful comments. Simulation results are available from the data base PANGAEA (doi: 10.1594/PANGAEA.868739).

References

Andres R, Boden T and Marland G 2015 *Annual Fossil-Fuel CO_2 Emissions: Global Stable Carbon Isotopic Signature* Carbon Dioxide Information Analysis Center, Oak Ridge National Laboratory, U.S. Department of Energy Oak Ridge, Tenn, USA (http://cdiac.ornl.gov/ndps/db1013_v2015.html)

Andres R, Marland G, Boden T and Bischof S 2000 Carbon dioxide emissions from fossil fuel consumption and cement manufacture, 1751–1991, and an estimate of their isotopic composition and latitudinal distribution *The Carbon Cycle* ed T Wigley and D Schimel (Cambridge: Cambridge University Press) pp 53–62

Bauska T K, Joos F, Mix A C, Roth R, Ahn J and Brook E J 2015 Links between atmospheric carbon dioxide, the land carbon reservoir and climate over the past millennium *Nat. Geosci.* **8** 383–7

Caldeira K, Rau G H and Duffy P B 1998 Predicted net efflux of radiocarbon from the ocean and increase in atmospheric radiocarbon content *Geophys. Res. Lett.* **25** 3811–4

Cao L and Caldeira K 2010 Atmospheric carbon dioxide removal: long-term consequences and commitment *Environ. Res. Lett.* **5** 024011

Eggleston S, Schmitt J, Bereiter B, Schneider R and Fischer H 2016 Evolution of the stable carbon isotope composition of atmospheric CO_2 over the last glacial cycle *Paleoceanography* **31** 434–52

Graven H D 2015 Impact of fossil fuel emissions on atmospheric radiocarbon and various applications of radiocarbon over this century *Proc. Natl Acad. Sci.* **112** 9542–5

Graven H D and Gruber N 2011 Continental-scale enrichment of atmospheric $^{14}CO_2$ from the nuclear power industry: potential impact on the estimation of fossil fuel-derived CO_2 *Atmos. Chem. Phys.* **11** 12339–49

Griffioen J 2016 Enhanced weathering of olivine in seawater: the efficiency as revealed by thermodynamic scenario analysis *Sci. Total Environ.* in press (doi:10.1016/j.scitotenv.2016.09.008)

Gruber N, Keeling C D, Bacastow R B, Guenther P R, Luecker T J, Wahlen M, Meijer H A J, Mook W G and Stocker T F 1999 Spatiotemporal patterns of carbon-13 in the global surface oceans and the oceanic Suess effect *Glob. Biogeochem. Cycles* **13** 307–35

Hauck J, Köhler P, Wolf-Gladrow D A and Völker C 2016 Iron fertilisation and century-scale effects of open ocean dissolution of olivine in a simulated CO_2 removal experiment *Environ. Res. Lett.* **11** 024007

Houghton R A 2003 Revised estimates of the annual net flux of carbon to the atmosphere from changes in land use and land management 1850-2000 *Tellus* **55B** 378–90

Hua Q, Barbetti M and Rakowski A Z 2013 Atmospheric radiocarbon for the period 1950–2010 *Radiocarbon* **55** 2059–72

Iyer G C *et al* 2015 The contribution of Paris to limit global warming to 2 °C *Environ. Res. Lett.* **10** 125002

Jahn A, Lindsay K, Giraud X, Gruber N, Otto-Bliesner B L, Liu Z and Brady E C 2015 Carbon isotopes in the ocean model of the Community Earth System Model (CESM1) *Geosci. Model Dev.* **8** 2419–34

Keeling C D 1979 The Suess effect: ^{13}Carbon-^{14}Carbon interrelations *Environ. Int.* **2** 229–300

Keeling C D, Bollenbacher A F and Whorf T P 2001 Exchanges of atmospheric CO_2 and $^{13}CO_2$ with the terrestrial biosphere and oceans from 1978 to 2000 *I. Global aspects, SIO Reference Series, No. 01-06* Scripps Institution of Oceanography, San Diego 88 pp

Keeling C D and Whorf T P 2005 Atmospheric CO_2 records from sites in the SIO air sampling network *Trends: A Compendium of Data on Global Change* Carbon Dioxide Information Analysis Center, Oak Ridge National Laboratory, U.S. Department of Energy, Oak Ridge, Tenn, USA

Knutti R, Rogelj J, Sedlacek J and Fischer E M 2016 A scientific critique of the two-degree climate change target *Nat. Geosci.* **9** 13–8

Köhler P, Abrams J F, Völker C, Hauck J and Wolf-Gladrow D A 2013 Geoengineering impact of open ocean dissolution of olivine on atmospheric CO_2, surface ocean pH and marine biology *Environ. Res. Lett.* **8** 014009

Köhler P, Fischer H, Munhoven G and Zeebe R E 2005 Quantitative interpretation of atmospheric carbon records over the last glacial termination *Glob. Biogeochem. Cycles* **19** GB4020

Köhler P, Hartmann J and Wolf-Gladrow D A 2010 Geoengineering potential of artificially enhanced silicate weathering of olivine *Proc. Natl Acad. Sci.* **107** 20228–33

Köhler P, Hauck J, Völker C and Wolf-Gladrow D 2015 Interactive comment on a simple model of the anthropogenically forced CO_2 cycle *Earth Syst. Dyn. Discuss.* **6** C813 (www.earth-syst-dynam-discuss.net/6/C813/2015/esdd-6-C813-2015.pdf)

Köhler P, Muscheler R and Fischer H 2006 A model-based interpretation of low frequency changes in the carbon cycle during the last 120,000 years and its implications for the reconstruction of atmospheric $\Delta^{14}C$ *Geochem. Geophys. Geosyst.* **7** Q11N06

Le Quéré C C *et al* 2015 Global carbon budget 2015 *Earth Syst. Sci. Data* **7** 349–96

Lloyd J and Farquhar G D 1994 ^{13}C discrimination during CO_2 assimilation by the terrestrial biosphere *Oecologia* **99** 201–15

Meinshausen M *et al* 2011 The RCP greenhouse gas concentrations and their extensions from 1765 to 2300 *Clim. Change* **109** 213–41

Meyerholt J, Zaehle S and Smith M J 2016 Variability of projected terrestrial biosphere responses to elevated levels of atmospheric CO_2 due to uncertainty in biological nitrogen fixation *Biogeosciences* **13** 1491–518

Moss R H *et al* 2010 The next generation of scenarios for climate change research and assessment *Nature* **463** 747–56

Naegler T and Levin I 2006 Closing the global radiocarbon budget 1945–2005 *J. Geophys. Res.* **111** D12311

Peterson C D, Lisiecki L E and Stern J V 2014 Deglacial whole-ocean $\delta^{13}C$ change estimated from 480 benthic foraminiferal records *Paleoceanography* **29** 549–63

Reimer P J *et al* 2013 IntCal13 and Marine13 radiocarbon age calibration curves 0–50,000 years cal BP *Radiocarbon* **55** 1869–87

Ridgwell A J 2001 Glacial-interglacial perturbations in the global carbon cycle *PhD Thesis* University of East Anglia Norwich, UK

Rogelj J, McCollum D L, O'Neill B C and Riahi K 2013 2020 emissions levels required to limit warming to below 2°C *Nat. Clim. Change* **3** 405–12

Rogelj J, Schaeffer M, Meinshausen M, Knutti R, Alcamo J, Riahi K and Hare W 2015 Zero emission targets as long-term global goals for climate protection *Environ. Res. Lett.* **10** 105007

Ronge T, Tiedemann R, Lamy F, Köhler P, Alloway B V, Pol-Holz R, Pahnke K, Southon J and Wacker L 2016 Radiocarbon constraints on the extent and evolution of the Pacific glacial carbon pool *Nat. Commun.* **7** 11487

Roth R and Joos F 2013 A reconstruction of radiocarbon production and total solar irradiance from the Holocene ^{14}C and CO_2 records: implications of data and model uncertainties *Clim. Past* **9** 1879–909

Rubino M *et al* 2013 A revised 1000-year atmospheric $\delta^{13}C$-CO_2 record from Law Dome and South Pole, Antarctica *J. Geophys. Res.: Atmos.* **118** 8482–99

Schmittner A, Gruber N, Mix A C, Key R M, Tagliabue A and Westberry T K 2013 Biology and air-sea gas exchange controls on the distribution of carbon isotope ratios ($\delta^{13}C$) in the ocean *Biogeosciences* **10** 5793–816

Smith K W, Reed S C, Cleveland C C, Ballantyne A P, Anderegg W R L, Wieder W R, Liu Y Y and Running S W 2016a Large divergence of satellite and Earth system model estimates of global terrestrial CO_2 fertilization *Nat. Clim. Change* **6** 306–10

Smith P *et al* 2016b Biophysical and economic limits to negative CO_2 emissions *Nat. Clim. Change* **6** 42–50

Stott L, Southon J, Timmermann A and Koutavas A 2009 Radiocarbon age anomaly at intermediate water depth in the Pacific Ocean during the last deglaciation *Paleoceanography* **24** A2223

Stuiver M and Quay P D 1981 Atmospheric ^{14}C changes resulting from fossil fuel CO_2 release and cosmic ray flux variability *Earth Planet. Sci. Lett.* **53** 349–62

Suess H E 1955 Radiocarbon concentration in modern wood *Science* **122** 415–7

Swart P K, Greer L, Rosenheim B E, Moses C S, Waite A J, Winter A, Dodge R E and Helmle K 2010 The ^{13}C Suess effect in scleractinian corals mirror changes in the anthropogenic CO_2 inventory of the surface oceans *Geophys. Res. Lett.* **37** L05604

Tagliabue A and Bopp L 2008 Towards understanding global variability in ocean carbon-13 *Glob. Biogeochem. Cycles* **22** GB1025

van Vuuren D P *et al* 2011 The representative concentration pathways: an overview *Clim. Change* **109** 5–31

Zeebe R E and Wolf-Gladrow D A 2001 *CO_2 in Seawater: Equilibrium, Kinetics, Isotopes* (*Elsevier Oceanography Book Series* vol 65) (Amsterdam: Elsevier)

Supplementary Material to
Using the Suess effect on the stable carbon isotope to distinguish the future from the past in radiocarbon

Peter Köhler

Alfred-Wegener-Institut Helmholtz-Zentrum für Polar-und Meeresforschung (AWI),
P.O. Box 12 01 61, 27515 Bremerhaven, Germany

E-mail: `Peter.Koehler@awi.de`

Model Description

In this study I use the well tested Box model of the Isotopic Carbon cYCLE (BICYCLE), which has been applied in several case studies on impacts of both natural and anthropogenic climate change on the evolution of the global carbon cycle (Köhler et al. 2005, Köhler, Hartmann & Wolf-Gladrow 2010). The model consists of a scheme, how prescribed changes in the physics of the climate system, e.g. ocean circulation, sea ice coverage, temperature, external input of the micro-nutrient iron, lead to variations in carbon fluxes between the various reservoirs, including changes in the carbon pumps that bring C and associated nutrients from the surface to the deep ocean and therefore to variable carbon budgets. Within the 10 oceanic, 1 atmospheric and 7 terrestrial boxes of the model not only C content, but also both its isotopic signatures, ^{13}C, ^{14}C, are traced. Furthermore, in the ocean total alkalinity, oxygen and PO_4^{3-} concentration are state variables, that change due to the variable physical boundary conditions. The model also consists of a simplistic scheme how terrestrial carbon content in vegetation and soil pool might alter due to a changing global temperature and atmospheric CO_2 concentration and considers differences in isotopic fractionation due to C_3 or C_4 photosynthesis. The terrestrial scheme is neglecting permafrost and peatland carbon pools and is not spatially resolved, thus it might only act to guide some very simplistic zero order changes in the carbon distribution between land, atmosphere, and ocean. However, it has been shown recently (Köhler et al. 2015) that the CO_2 fertilization which might be realized within such a simple scheme of the terrestrial biosphere leads to much too high land carbon uptake for some RCP emissions scenarios. I therefore restrict my analysis in the following to an atmosphere-ocean only system by keeping the terrestrial carbon content constant, but I will show some results including the dynamical terrestrial biosphere for the historical period.

BICYCLE also contains a time-delayed response function of changes in deep ocean carbonate ion concentration, that mimics the carbonate compensation effect (Broecker & Peng 1987), which is the response of the deep ocean - sediment fluxes of carbonate dissolution / accumulation to any changes in the carbon cycle. The impact of the carbonate compensation is on the time scales of interest (some centuries) small (simulated atmospheric CO_2 varies by less than 1%), but the process is included here for the sake of completeness.

Since my model-setup does not contain the physical part of the climate system, the global temperature change ΔT (relevant for both atmosphere–ocean gas exchange and the turnover time of carbon in terrestrial reservoirs) connected with a change in atmospheric CO_2 is calculated using the transient climate sensitivity (TCS) for CO_2 doubling, which has been obtained from more sophisticated climate models, and which has been recalculated to TCS = 2 K recently by a data-based approach (Storelvmo et al. 2016). In detail, I calculate $\Delta T = \mathrm{TCS} \times \Delta R_{\mathrm{CO_2}}/\Delta R_{2\times\mathrm{CO_2}}$ with $\Delta R_{\mathrm{CO_2}} = 5.35\ \mathrm{W/m^2} \cdot \ln(\mathrm{CO_2}/278\ \mathrm{ppmv})$ (Myhre et al. 1998). Changes in sea surface temperature (SST) are assumed to follow ΔT and changing SST will influence via Henry's Law the CO_2 solubility in the ocean and isotopic fractionation during gas exchange (Zeebe & Wolf-Gladrow 2001).

The simulated time period contains the bomb spike in ^{14}C in the second half of the 20th century and the depletion in both $\delta^{13}C$ and $\Delta^{14}C$ according to the historical Suess effects. In order to match observed variations in $\Delta^{14}C$ as good as possible the ^{14}C production rate is prescribed from (Roth & Joos 2013) varying around a mean production rate of 440 mol per year (Fig. S1C). The previous study (Graven 2015) also considered ^{14}C production from the nuclear industry with assumed ^{14}C emissions being constant at the 2005 level following a recent inventory (Graven & Gruber 2011). These nuclear industry ^{14}C emissions were shown to be on the order of 10% of the natural ^{14}C production rate. Here, I refrain from assuming any ^{14}C emissions from nuclear industry, since its evolution in the future is difficult to propose. However, I estimate the size of its impact on the ^{14}C cycle in BICYCLE in a sensitivity run, in which for RCP8.5 ^{14}C production rate gradually rose from year 1980 onward to +10% in year 2005 CE (or to a relative ^{14}C production rate of 1.1), and constant thereafter (Fig. S1C). The simulated atmospheric $\Delta^{14}C$ based on this revised ^{14}C production rate was 5‰ and 10‰ higher in year 2100 and 2500, respectively. Also note that the reconstructed size of the ^{14}C emission from the nuclear industry is on the same order of magnitude as the variation in the natural ^{14}C production rate in the industrial period (Fig. S1C), but smaller than its variability over the last 10,000 years (Roth & Joos 2013).

All simulations are started in year 10,000 BP to allow the ^{14}C cycle to adjust to variable production rates. From 1950 CE onward the ^{14}C production rate is kept constant, but was perturbed in individual years of the 1950ies to 1970ies by high peaks in ^{14}C production caused by nuclear bomb testing (Naegler & Levin 2006) (Fig. S1C). The cumulative bomb-^{14}C production leads to the injection of $1.2 \cdot 10^6$ g ^{14}C into the atmosphere after 1950, 15% smaller than suggested, because the natural background ^{14}C production

rate in BICYCLE is also only 85% of that chosen previously (Naegler & Levin 2006).

Model Evaluation

For evaluation of the model performance in the historical period (Fig. S2) dynamics of ^{14}C in the time windows 1820–1950 (historical ^{14}C Suess effect) and 1950–2010 (bomb-^{14}C) have to be distinguished, since the impact of the Suess effect on ^{14}C is after 1950 superimposed by bomb-^{14}C.

The time window 1820–1950 covers the full data set of one of the first reconstructions of the ^{14}C Suess effect from tree ring data (Stuiver & Quay 1981). In this period all atmospheric carbon variables using a constant terrestrial biosphere (experiment TB–; my standard setup) have a small offset in the simulations from the data (Fig. S2), while their dynamic trends meet the evolution seen within the data: CO_2 rises by 30–35 ppmv, $\delta^{13}C$ falls by 0.6–0.7‰, $\Delta^{14}C$ falls by 20–25‰ after year 1900 superimposed on some decadal-scale variability, which was probably caused by changes in the ^{14}C production rate (Roth & Joos 2013). The carbon cycle dynamics of the data are even better met by the model simulations which includes an active terrestrial biosphere (experiment TB+ in Fig. S2): a slightly smaller rise in CO_2, smaller decrease of $\delta^{13}C$ more in line with the data, and hardly any offset in $\Delta^{14}C$.

In the 60 years including the bomb radiocarbon (1950–2010) the simulated CO_2 rises by 108 ppmv in experiment TB–, which is more than the observed rise by 80 ppmv (Fig. S2), but well within the uncertainty band of the C^4MIP results (Friedlingstein et al. 2006). This offset is certainly caused by the fixed terrestrial carbon pools in my setup. In scenarios with active terrestrial biosphere simulated CO_2 rises by 71 ppmv between 1950 and 2010, agreeing with the lower range of the C^4MIP range of results. In the historical period the land carbon is the least known pool and its change is typically derived from the residual after observed and modeled change in atmosphere and ocean have been subtracted from the anthropogenic emissions and during the historical period this residual land carbon sink took up about a fourth of the emissions (Le Quéré et al. 2015). The decreasing trend in simulated atmospheric $\delta^{13}C$ was with -2.12‰ in TB+ larger than the decrease of about -1.4‰ in the data (Fig. S2B). This model-data mismatch is also caused by the missing terrestrial carbon sink, since the simulated trend of -1.16‰ in atmospheric $\delta^{13}C$ in TB– agrees better with the trend in the data. Since simulated CO_2 in the long term agrees reasonable well with CMIP5 data (Figs. 1D, 2C) I judge this misfit in atmospheric $\delta^{13}C$ to be only of minor importance for the overall conclusions.

The global mean atmospheric $\Delta^{14}C$ peaks in the data in the mid 1960s at 700 ± 200‰ and declines towards +50‰ in year 2010 thereafter. The simulated peak in bomb-^{14}C is with +900‰ at the upper end of the range of reconstructions, decaying thereafter to +5‰ in year 2010 (Fig. S2C). The decay of the $\Delta^{14}C$ peak in atmosphere is faster in the model than in the data which indicates that the vertical mixing between surface and deep ocean in the model operates faster than in nature. This is a phenomenon well known for box models, but less pronounced in BICYCLE than in other box models (Köhler et al. 2005, Broecker et al. 1999).

Simulated ocean acidification represented by a fall in surface ocean pH is difficult to compare with data, because observations exist only for a few sites since about 1990 (Doney et al. 2009). Nevertheless, the decline of ∼0.02 pH units per decade over less than 20 years detected in these data is in agreement with the BICYCLE simulations shown here (Fig. 1G). The time series of the pH data are so short that I do not show them in the figures.

One integrated approach to evaluate my model performance is to plot the calculated temperature change ΔT as a function of cumulative CO_2 emission (Fig. S3). When compared with CMIP5 results, which are here restricted to scenarios with CO_2 emissions only (neglecting global warming connected with anthropogenic emissions of CH_4, N_2O, or any aerosol effects) I find my box model simulations very well in the middle of the uncertainty range spanned by simulation results of the Earth system models (ESM) contributing to CMIP5. Until the year 2100 I would find in RCP8.5 (about 2500 PgC of cumulative CO_2 emissions) a warming of 4 K, which rises to a maximum of 5.7 K for the cumulative CO_2 emissions of 5300 PgC. The slight decline towards 5.5 K for even higher cumulative CO_2 emissions (nearly 6000 PgC) is due to the small annual emission rate of 1.5 Pg C yr^{-1} during the last 250 simulated years within RCP8.5 which allows the ocean to absorb more CO_2 than is emitted, therefore lowering atmospheric CO_2 and global warming. Also note, that in my simple modeling approach ΔT is not a linear function of cumulative CO_2 emission (Fig. S3). Such a non-linear relationship between ΔT and cumulative CO_2 emission has already been found for results based on Earth system models of intermediate complexity (EMICs) (Allen et al. 2009), while state-of-the-art ESM contributing to CMIP5 find this relationship to be rather linear, not only for the 21st century (IPCC 2013), but also for cumulative emissions up to 5000 PgC (Tokarska et al. 2016). For comparing my simple carbon cycle model with these results based on more complex models, one needs to be aware that no warming beyond that caused by CO_2 is contained in my results. Furthermore, it is even not yet clear why the results based on ESMs and EMICs differ for high cumulative CO_2 emissions (Frölicher 2016).

Another evaluation method for carbon cycle models is the simulation of a CO_2 pulse response (Joos et al. 2013). The model response to the instantaneous injection of 100 PgC into the atmosphere for modern background conditions (here: atmospheric CO_2 concentration of 389 ppmv) is then investigated. The airborne fraction f of this CO_2 pulse decays over time. In my atmosphere-ocean version of the BICYCLE model with constant terrestrial biosphere I find f of 0.45 after one century to decline towards 0.20 after one millennium, well in agreement with results from more complex models ($f = 0.41 \pm 0.13$ (2σ) and $f = 0.25 \pm 0.09$ after 100 and 1000 years, respectively) which contributed to the intercomparison study (Joos et al. 2013).

If compared directly with the previous study (Graven 2015) one needs to keep in mind that here the whole carbon cycle including the carbon isotopes are freely evolving in response to changing boundary conditions (implying that I prescribe natural and bomb-^{14}C production of radiocarbon), while in the previous approach the measured atmospheric $\Delta^{14}C$ data for the historical period have been prescribed. As result of this difference in the

setup, I am here able to compare simulated Δ^{14}C with data for the past to test the model performance, while this is *per se* not possible in Graven (2015). The radiocarbon age and the corresponding atmospheric Δ^{14}C in year 2100 are in my simulations 2343 years (−253‰) in RCP8.5, 1516 years (−172‰) in RCP6.0, 758 years (−90‰) in RCP4.5 and 261 years (−32‰) in RCP2.6. My simulated age for RCP2.6 is slightly older (Δ^{14}C smaller) than in (Graven 2015), while all other results agree well with this previous study. All-together, I conclude that both modeling approaches are similar in complexity and produce comparable results.

References

Allen M R, Frame D J, Huntingford C, Jones C D, Lowe J A, Meinshausen M & Meinshausen N 2009 Warming caused by cumulative carbon emissions towards the trillionth tonne *Nature* **458**(7242), 1163–1166.

Andres R, Boden T & Marland G 2015 Annual Fossil-Fuel CO_2 Emissions: Global Stable Carbon Isotopic Signature *in* 'Carbon Dioxide Information Analysis Center' Oak Ridge National Laboratory, U.S. Department of Energy Oak Ridge, Tenn., U.S.A.

Andres R, Marland G, Boden T & Bischof S 2000 Carbon dioxide emissions from fossil fuel consumption and cement manufacture, 1751-1991, and an estimate of their isotopic composition and latitudinal distribution *in* T Wigley & D Schimel, eds, 'The Carbon Cycle' Cambridge University Press Cambridge pp. 53–62.

Bauska T K, Joos F, Mix A C, Roth R, Ahn J & Brook E J 2015 Links between atmospheric carbon dioxide, the land carbon reservoir and climate over the past millennium *Nature Geoscience* **8**(5), 383–387.

Broecker W, Lynch-Stieglitz J, Archer D, Hofmann M, Maier-Reimer E, Marchal O, Stocker T & Gruber N 1999 How strong is the Harvardton-Bear constraint? *Global Biogeochemical Cycles* **13**(4), 817–820.

Broecker W S & Peng T H 1987 The role of $CaCO_3$ compensation in the glacial to interglacial atmospheric CO_2 change *Global Biogeochemical Cycles* **1**, 15–29.

Doney S C, Fabry V J, Feely R A & Kleypas J A 2009 Ocean acidification: the other CO_2 problem *Annual Review of Marine Science* **1**, 169–192.

Friedlingstein P, Cox P, Betts R, Bopp L, von Bloh W, Brovkin V, Cadule P, Doney S, Eby, Fung I, Bala G, John J, Joos F, Kato T, Kawamiya M, Knorr W, Lindsay K, Matthews H D, Raddatz T, Rayner P, Reick C, Roeckner E, Schnitzler K G, Schnur R, Strassmann K, Weaver A J, Yoshikawa C & Zeng N 2006 Climate-carbon cycle feedback analysis: results from the C^4MIP model intercomparison *Journal of Climate* **19**, 3337–3353.

Frölicher T L 2016 Climate response: Strong warming at high emissions *Nature Climate Change* **6**, 823–824.

Graven H D 2015 Impact of fossil fuel emissions on atmospheric radiocarbon and various applications of radiocarbon over this century *Proceedings of the National Academy of Sciences* **112**(31), 9542–9545.

Graven H D & Gruber N 2011 Continental-scale enrichment of atmospheric $^{14}CO_2$ from the nuclear power industry: potential impact on the estimation of fossil fuel-derived CO_2 *Atmospheric Chemistry and Physics* **11**(23), 12339–12349.

Hua Q, Barbetti M & Rakowski A Z 2013 Atmospheric radiocarbon for the period 1950-2010 *Radiocarbon* **55**(4), 2059–2072.

IPCC 2013 Summary for Policymakers *in* T Stocker, D Qin, G.-K Plattner, M Tignor, S Allen, J Boschung, A Nauels, Y Xia, V Bex & P Midgley, eds, 'Climate Change 2013: The Physical Science Basis. Contribution of Working Group I to the Fifth Assessment Report of

the Intergovernmental Panel on Climate Change' Cambridge University Press Cambridge, United Kingdom and New York, NY, USA pp. 3–29.

Joos F, Roth R, Fuglestvedt J S, Peters G P, Enting I G, von Bloh W, Brovkin V, Burke E J, Eby M, Edwards N R, Friedrich T, Frölicher T L, Halloran P R, Holden P B, Jones C, Kleinen T, Mackenzie F T, Matsumoto K, Meinshausen M, Plattner G K, Reisinger A, Segschneider J, Shaffer G, Steinacher M, Strassmann K, Tanaka K, Timmermann A & Weaver A J 2013 Carbon dioxide and climate impulse response functions for the computation of greenhouse gas metrics: a multi-model analysis *Atmospheric Chemistry and Physics* **13**(5), 2793–2825.

Keeling C D, Piper S C, Bacastow R B, Wahlen M, Whorf T P, Heimann M & Meijer H A 2001 Exchanges of atmospheric CO_2 and $^{13}CO_2$ with the terrestrial biosphere and oceans from 1978 to 2000. I. Global aspects, SIO Reference Series, No. 01-06 Technical report Scripps Institution of Oceanography San Diego.

Keeling C D & Whorf T P 2005 Atmospheric CO_2 records from sites in the SIO air sampling network *in* 'Trends: A Compendium of Data on Global Change' Carbon Dioxide Information Analysis Center, Oak Ridge National Laboratory, U.S. Department of Energy, Oak Ridge, Tenn., USA.

Köhler P, Fischer H, Munhoven G & Zeebe R E 2005 Quantitative interpretation of atmospheric carbon records over the last glacial termination *Global Biogeochemical Cycles* **19**, GB4020.

Köhler P, Fischer H & Schmitt J 2010 Atmospheric $\delta^{13}CO_2$ and its relation to pCO_2 and deep ocean $\delta^{13}C$ during the late Pleistocene *Paleoceanography* **25**, PA1213.

Köhler P, Hartmann J & Wolf-Gladrow D A 2010 Geoengineering potential of artificially enhanced silicate weathering of olivine *Proceedings of the National Academy of Science* **107**(47), 20228–20233.

Köhler P, Hauck J, Völker C & Wolf-Gladrow D 2015 Interactive comment on *A simple model of the anthropogenically forced CO_2 cycle* by W. Weber et al. *Earth System Dynamics Discussions* **6**, C813, http://www.earth–syst–dynam–discuss.net/6/C813/2015/.

Köhler P, Muscheler R & Fischer H 2006 A model-based interpretation of low frequency changes in the carbon cycle during the last 120 000 years and its implications for the reconstruction of atmospheric $\Delta^{14}C$ *Geochemistry, Geophysics, Geosystems* **7**, Q11N06.

Le Quéré C, Moriarty R, Andrew R M, Canadell J G, Sitch S, Korsbakken J I, Friedlingstein P, Peters G P, Andres R J, Boden T A, Houghton R A, House J I, Keeling R F, Tans P, Arneth A, Bakker D C E, Barbero L, Bopp L, Chang J, Chevallier F, Chini L P, Ciais P, Fader M, Feely R A, Gkritzalis T, Harris I, Hauck J, Ilyina T, Jain A K, Kato E, Kitidis V, Klein Goldewijk K, Koven C, Landschützer P, Lauvset S K, Lefèvre N, Lenton A, Lima I D, Metzl N, Millero F, Munro D R, Murata A, Nabel J E M S, Nakaoka S, Nojiri Y, O'Brien K, Olsen A, Ono T, Pérez F F, Pfeil B, Pierrot D, Poulter B, Rehder G, Rödenbeck C, Saito S, Schuster U, Schwinger J, Séférian R, Steinhoff T, Stocker B D, Sutton A J, Takahashi T, Tilbrook B, van der Laan-Luijkx I T, van der Werf G R, van Heuven S, Vandemark D, Viovy N, Wiltshire A, Zaehle S & Zeng N 2015 Global Carbon Budget 2015 *Earth System Science Data* **7**(2), 349–396.

Meinshausen M, Smith S, Calvin K, Daniel J, Kainuma M, Lamarque J F, Matsumoto K, Montzka S, Raper S, Riahi K, Thomson A, Velders G & van Vuuren D 2011 The RCP greenhouse gas concentrations and their extensions from 1765 to 2300 *Climatic Change* **109**(1-2), 213–241.

Myhre G, Highwood E J, Shine K P & Stordal F 1998 New estimates of radiative forcing due to well mixed greenhouse gases *Geophysical Research Letters* **25**, 2715–2718.

Naegler T & Levin I 2006 Closing the global radiocarbon budget 1945-2005 *Journal of Geophysical Research* **111**, D12311, doi: 10.1029/2005JD006758.

Peterson C D, Lisiecki L E & Stern J V 2014 Deglacial whole-ocean $\delta^{13}C$ change estimated from 480 benthic foraminiferal records *Paleoceanography* **29**(6), 549–563.

Reimer P J, Bard E, Bayliss A, Beck J W, Blackwell P G, Bronk Ramsey C, Grootes P M, Guilderson T P, Haflidason H, Hajdas I, Hatté C, Heaton T J, Hoffmann D L, Hogg A G, Hughen K A, Kaiser K F, Kromer B, Manning S W, Niu M, Reimer R W, Richards D A, Scott E M, Southon J R, Staff R A, Turney C S M & van der Plicht J 2013 IntCal13 and Marine13 Radiocarbon Age Calibration Curves 0–50,000 Years cal BP *Radiocarbon* **55**(4), 1869–1887.

Roth R & Joos F 2013 A reconstruction of radiocarbon production and total solar irradiance from the

Holocene ^{14}C and CO_2 records: implications of data and model uncertainties *Climate of the Past* **9**(4), 1879–1909.

Rubino M, Etheridge D M, Trudinger C M, Allison C E, Battle M O, Langenfelds R L, Steele L P, Curran M, Bender M, White J W C, Jenk T M, Blunier T & Francey R J 2013 A revised 1000-year atmospheric $\delta^{13}C$-CO_2 record from Law Dome and South Pole, Antarctica *Journal of Geophysical Research: Atmospheres* **118**(15), 8482–8499.

Storelvmo T, Leirvik T, Lohmann U, Phillips P C B & Wild M 2016 Disentangling greenhouse warming and aerosol cooling to reveal Earth's climate sensitivity *Nature Geoscience* **9**(4), 286–289.

Stuiver M & Quay P D 1981 Atmospheric ^{14}C changes resulting from fossil fuel CO_2 release and cosmic ray flux variability *Earth and Planetary Science Letters* **53**, 349–362.

Tokarska K B, Gillett N P, Weaver A J, Arora V K & Eby M 2016 The climate response to five trillion tonnes of carbon *Nature Climate Change* **6**, 851–855.

Zeebe R E & Wolf-Gladrow D A 2001 *CO_2 in Seawater: Equilibrium, Kinetics, Isotopes* Vol. 65 of *Elsevier Oceanography Book Series* Elsevier Science Publishing Amsterdam, The Netherlands.

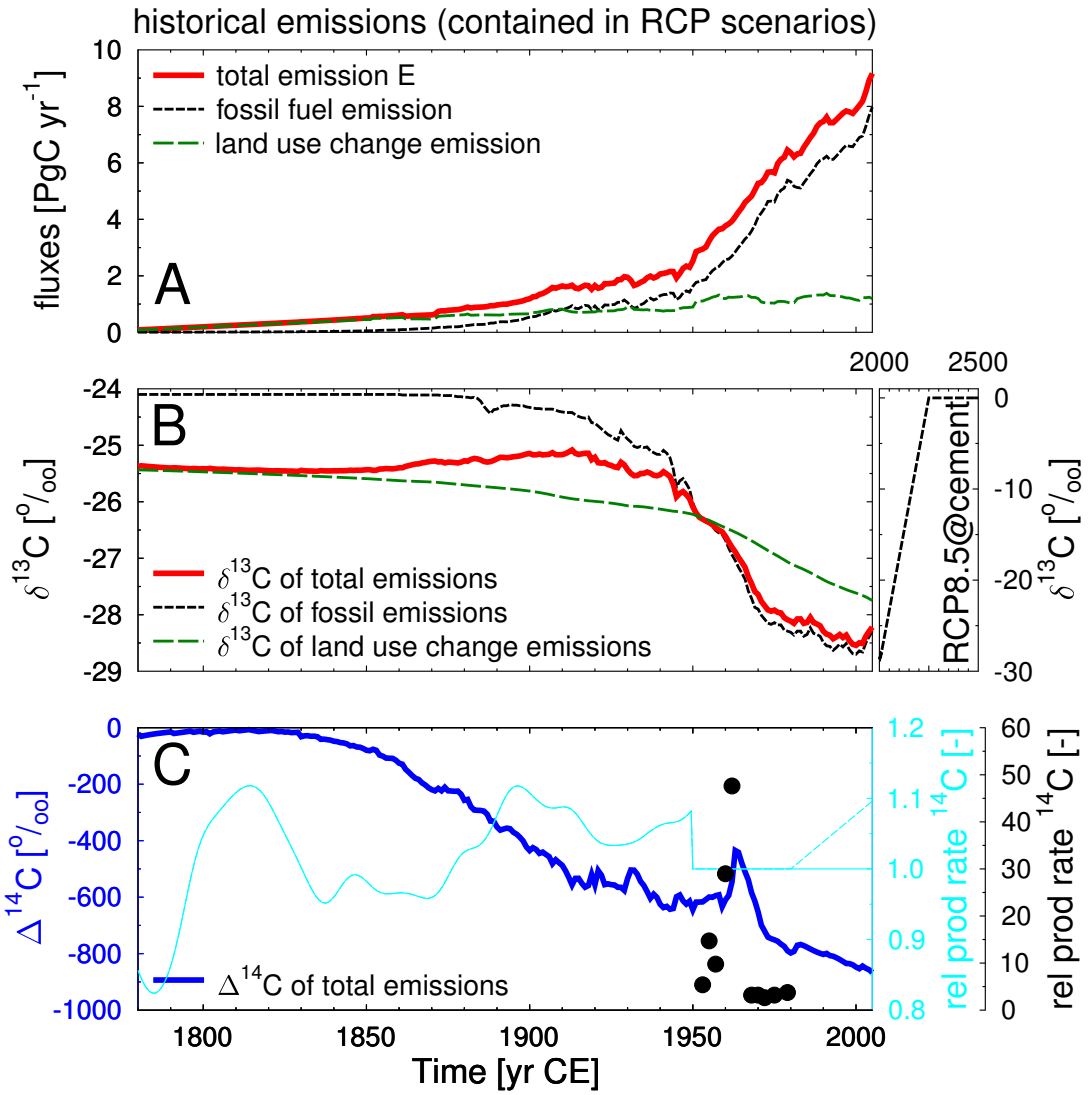

Figure S1: Detailed forcing of the historical simulations. A: Anthropogenic emissions, total and subdivided in those based on fossil fuels or land use change (Meinshausen et al. 2011). Note, that fossil fuel emissions also contains CO_2 release from cement production. B: The related δ^{13}C signatures of the land use change (internally calculated), fossil emissions (Andres et al. 2000, Andres et al. 2015) and the mean δ^{13}C of the total emission flux. Black broken line shows δ^{13}C signature of fossil fuel emissions following a gradually increase in cement production (to 100% in year 2250) in the fossil fuel source mix used in scenario RCP8.5@cement. C: Δ^{14}C of the total anthropogenic emissions and the relative change in the ^{14}C production rate (Roth & Joos 2013). Broken line (1980 – 2000) indicates a rise in ^{14}C production rate by 10% in the year 2005 (and constant thereafter) due to the nuclear industry (Graven & Gruber 2011), whose impact is tested in a sensitivity study. Dots in panel C are anthropogenic (bomb-based) increases in ^{14}C production rate derived from a closure of the ^{14}C cycle (Naegler & Levin 2006) on it own y-axis.

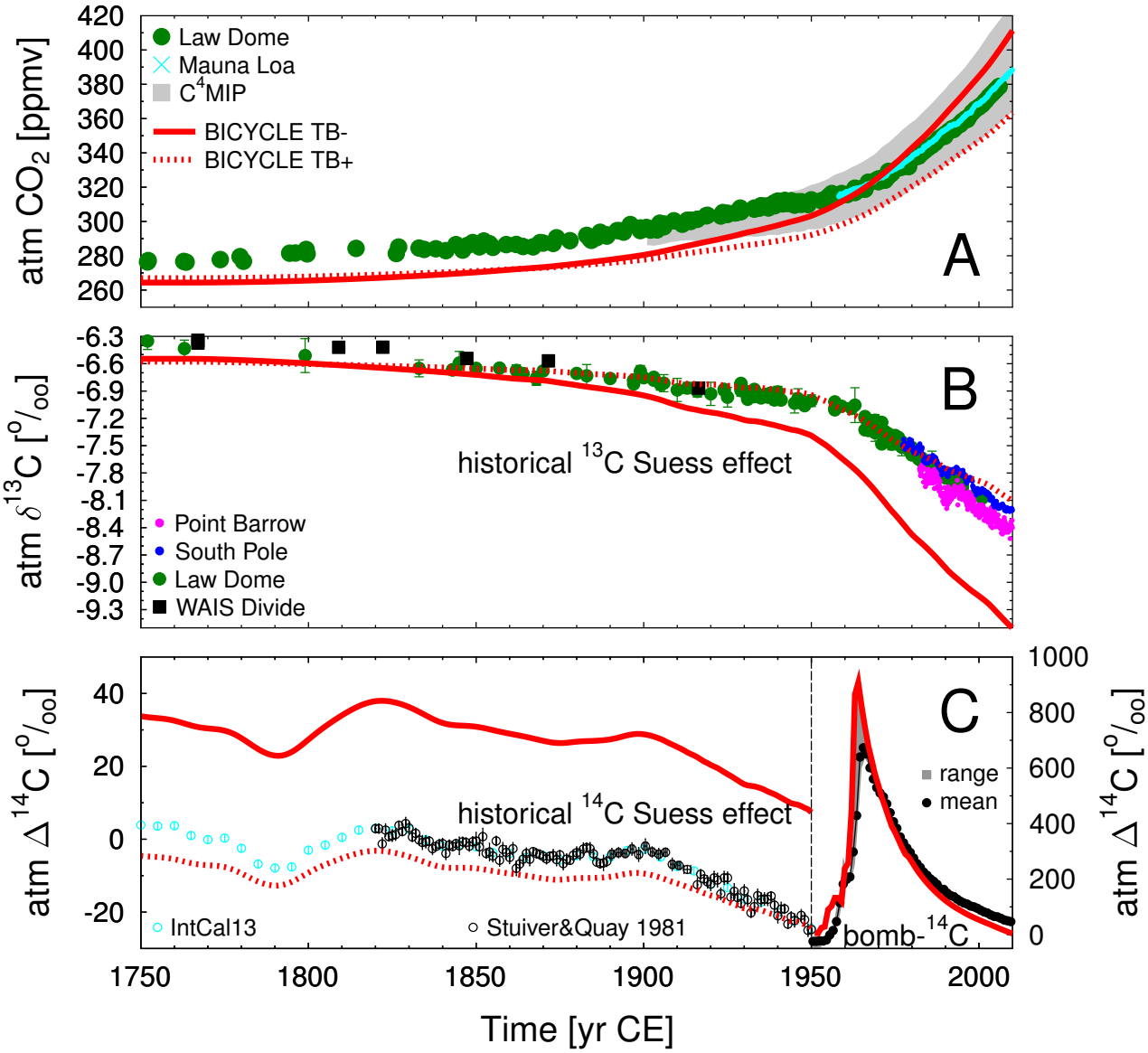

Figure S2: Evaluating the historical simulations. Comparing atmospheric (A) CO_2, (B) $\delta^{13}C$, (C) $\Delta^{14}C$ of historical simulations of the BICYCLE carbon cycle model with data. In the BICYCLE simulations the terrestrial biosphere is either passive (=constant) (TB–) or active (TB+). Vertical line in (C) indicates the break in the y-axis in $\Delta^{14}C$ at 1950 CE. CO_2: instrumental (Mauna Loa) (Keeling & Whorf 2005) and Law Dome ice core (Rubino et al. 2013); $\delta^{13}C$: instrumental (Point Barrow, South Pole) (Keeling et al. 2001), Law Dome and WAIS Divide ice cores (Rubino et al. 2013, Bauska et al. 2015); $\Delta^{14}C$: pre-bomb reconstructions of $\Delta^{14}C$ (IntCal13 (Reimer et al. 2013)) including the historical ^{14}C Suess effect (Stuiver & Quay 1981) and the ^{14}C-bomb peak (global mean and range) (Hua et al. 2013). Monthly mean data of the instrumental periods were aggregated into annual mean values.

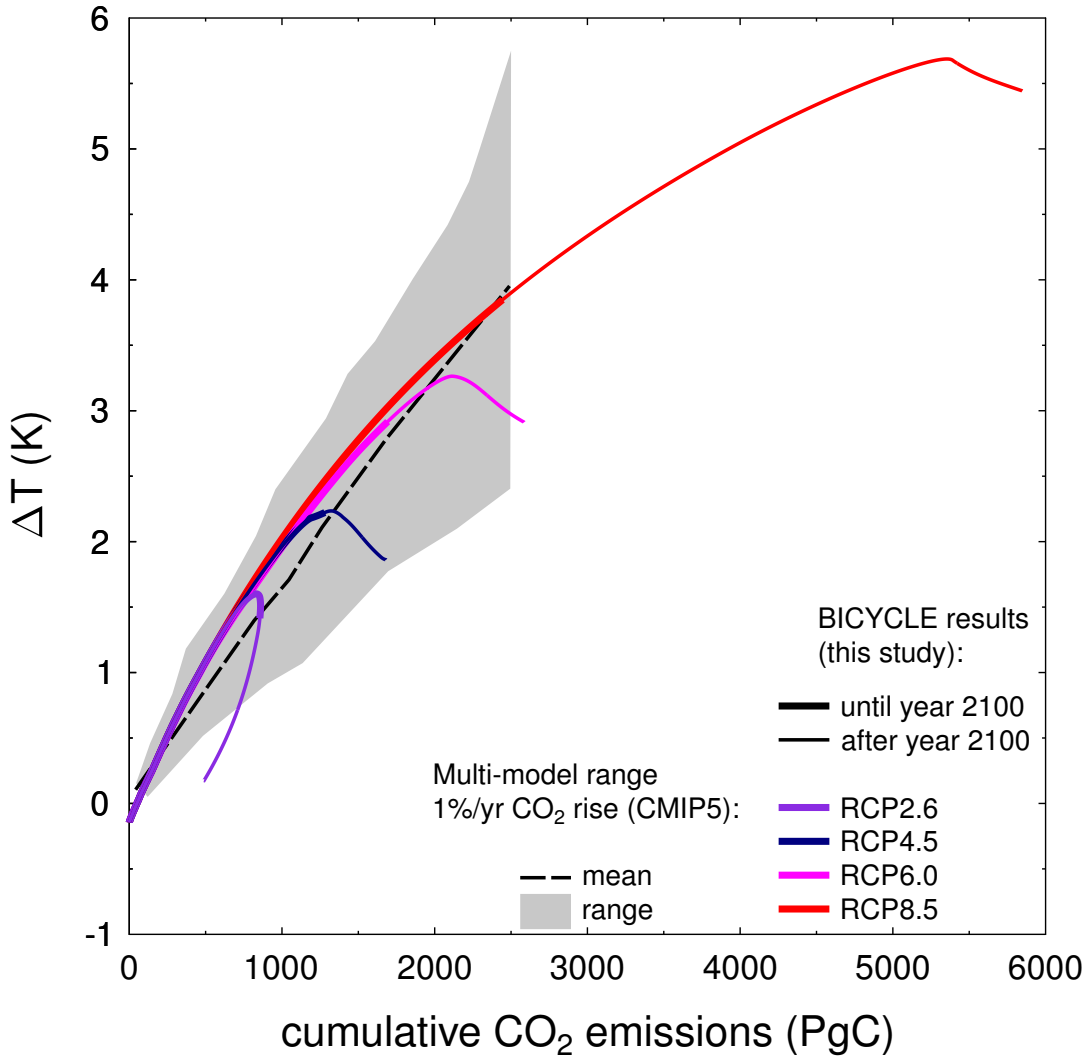

Figure S3: Global mean surface temperature increase as a function of cumulative global CO_2 emissions. Colored lines are own simulation results with the BICYCLE model for the four different RCP emission scenarios with passive terrestrial biosphere using the net CO_2 emissions. Simulation results show changes from the beginning of the emissions (year 1765) until year 2100 (thick lines), and thereafter (2101–2500, thin lines). For the BICYCLE results I directly calculate ΔT from CO_2 using a transient climate response of 2 K as given in the methods. For comparison the multi-model mean and range simulated by CMIP5 models, forced by a CO_2 increase of 1% per year is given by the broken black line and gray area (after Figure SPM 10 of (IPCC 2013)). These simulations exhibit lower warming than those driven by RCPs within CMIP5, which include additional non-CO_2 forcings and therefore lead to higher temperature changes. For the CMIP5 results ΔT until the year 2100 is calculated relative to the 1861–1880, CO_2 emissions relative to 1870.

Figure S4: Analysis of the combined Suess effects on both ^{14}C and ^{13}C for oceanic surface and deep reservoirs: (A) surface North Atlantic (same data as in Fig. 3B); (B) surface Equatorial Atlantic; (C) deep Atlantic; (D) surface Southern Ocean; (E) deep Southern Ocean; (F) surface North Pacific; (G) surface Equatorial Indo-Pacific; (H) deep Indo-Pacific (same data as in Fig. 3C). Here, deep ocean boxes are all water masses below 1000 m; surface water boxes are 100 m deep in the equatorial region and 1000 m deep in the high latitudes; North Atlantic (Pacific) is north of 50° N (40° N); Southern Ocean is south of 40° S. A more detailed description of the definition of the different reservoirs including water mass fluxes in found elsewhere (Köhler, Fischer & Schmitt 2010). Scatter plots of simulated $\Delta^{14}C$ versus $\delta^{13}C$ showing the historical and future Suess effect and the influence of bomb-^{14}C, future CO_2 emissions and carbon dioxide reduction (CDR) approaches (BECCS, DAC, EW) on both variables. Also included in dotted lines are results for RCP2.6, RCP4.5 and RCP6.0, which all contain a prescribed contribution of BECCS (see Fig. 1 for details). For comparison, also the available paleo knowledge is added. I show the data range obtained from sediment cores in deep ocean $\delta^{13}C$ (Peterson et al. 2014) for a fixed value of $\Delta^{14}C = 100‰$ obtained for the Last Glacial Maximum (LGM) and the late Holocene (HOL). For the surface ocean $\Delta^{14}C$ in Marine13 (Reimer et al. 2013) is plotted. Additionally, the range in both isotopes in previously published (imperfect) simulations using the BICYCLE model covering the last 50,000 year (50 ka) (upper limit of scenario S3x (^{14}C production rate based on ^{10}Be) and lower limit of scenario S4x (^{14}C production rate based on reconstructions of the geomagnetic field strength GLOPIS-75) as used before (Köhler et al. 2006)). The gray broken line in all subplots crosses values for year 2020 with a slope $m = 50$ (see text for further explanation).

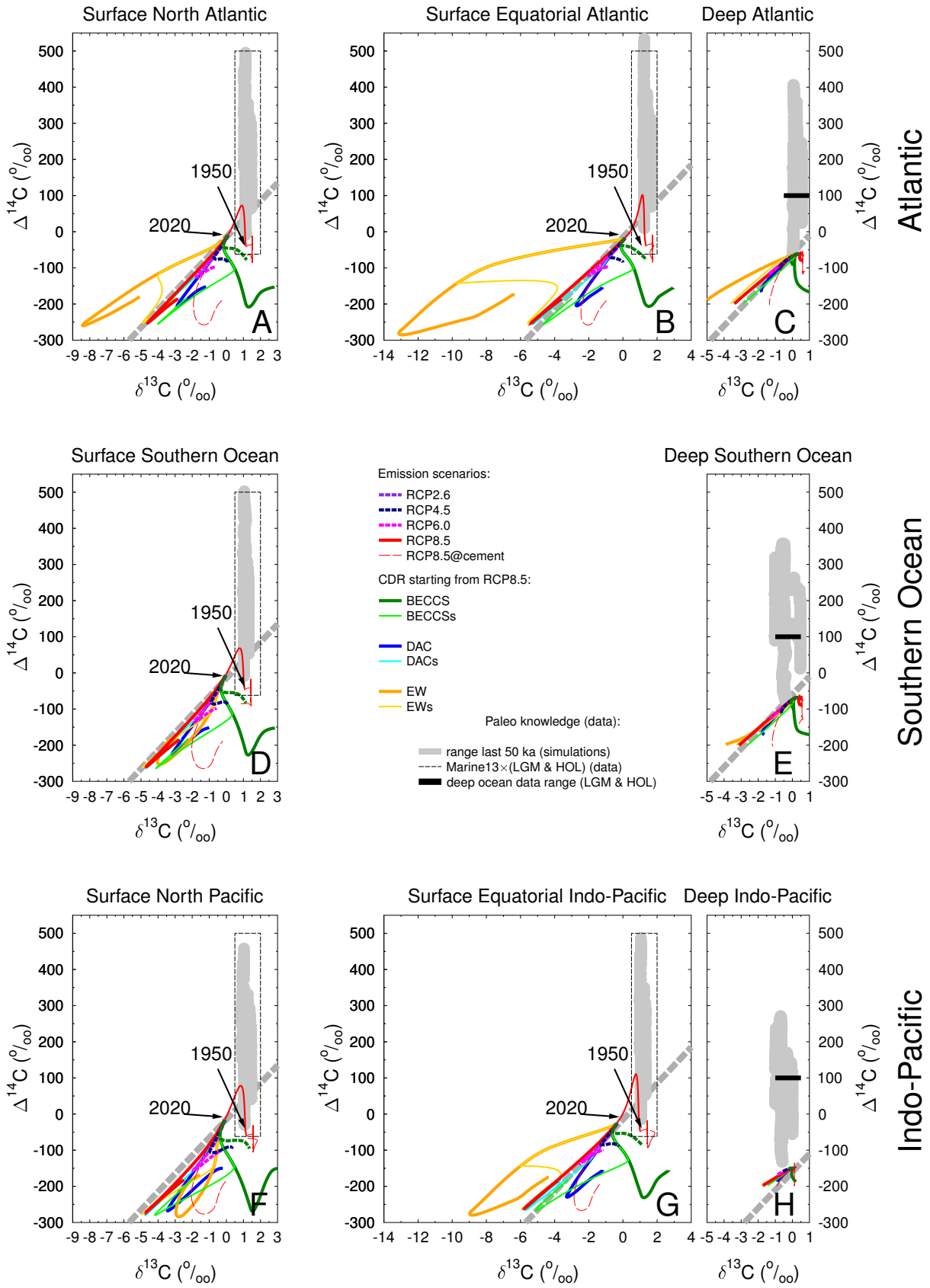

Figure S4: Caption on previous page.